Available online at www.sciencedirect.com
ScienceDirect
Biochimica et Biophysica Acta 1758 (2006) 942–947
BIOCHIMICA ET BIOPHYSICA ACTA
BBA
www.elsevier.com/locate/bbamem

Review

Infrared imaging microscopy of bone: Illustrations from a mouse model of Fabry disease

Adele L. Boskey [a,*], Michel Goldberg [b], Ashok Kulkarni [c], Santiago Gomez [d]

[a] *Hospital for Special Surgery and Weill Medical College of Cornell University*
[b] *Laboratoire Reparation et Remodelage des Tissus Oro-Faciaux, EA 4296, Groupe Matrices Extracellulaires et Biomineralisations, Faculte de Chirurgie Dentaire, Universite Paris V, Montrouge, France*
[c] *Functional Genomics Section, Craniofacial Developmental and Regeneration Biology Branch, National Institute of Dental and Cranial Research, National Institutes of Health, Bethesda, MD 20892, USA*
[d] *Departamento de Anatomia Patologica, University of Cadiz, Spain*

Received 11 January 2006; received in revised form 14 February 2006; accepted 16 February 2006
Available online 15 March 2006

Abstract

Bone is a complex tissue whose composition and properties vary with age, sex, diet, tissue type, health and disease. In this review, we demonstrate how infrared spectroscopy and infrared spectroscopic imaging can be applied to the study of these variations. A specific example of mice with Fabry disease (a lipid storage disease) is presented in which it is demonstrated that the bones of these young animals, while showing typical spatial variation in mineral content, mineral crystal size, and collagen maturity, do not differ from the bones of age- and sex-matched wild type animals.

Keywords: Infrared microscopic imaging; Bone; Hydroxyapatite; Fabry disease

Contents

1. Introduction

Bone is a dynamic tissue whose composition changes with development, environment, genetics, health and disease. The composition, architecture, and geometry all contribute to the mechanical integrity of the bone. While there are numerous techniques to determine overall geometry and density of human and mouse bones[1,2], fewer techniques exist that enable characterization of architectural variation in bone mineral and matrix composition [3]. We have used infrared microspectroscopy and infrared microscopic imaging to characterize both healthy bone and disease bone in humans and in animals [4]. Our methodology is based on analysis of parameters that have been used for infrared characterization of bone and tooth

* Corresponding author.
E-mail address: boskeya@hss.edu (A.L. Boskey).

0005-2736/$ - see front matter © 2006 Elsevier B.V. All rights reserved.
doi:10.1016/j.bbamem.2006.02.019

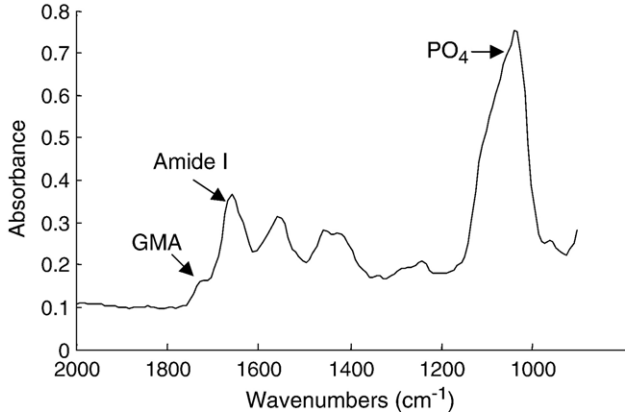

Fig. 1. Typical Infrared spectra from the central cortex of a normal (wildtype) 8 month old mouse tibia. The regions of interest are labeled.

mineral properties over almost the past century (for review, see [3–5]. This article summarizes the infrared spectroscopic methods used to study bone mineral changes in health and disease, with a specific example take from the study of a lipid storage disease in which globotriaosylceramide (Gb3) accumulates in tissues. To appreciate these analyses, it is important to first review the structure and function of bone.

2. Bone structure and function

The bones of the body are generally classified based on shape (long and flat), the mechanism by which they are formed, or the actual arrangement of the components. The long bones (like the femur and tibia) are tubes filled with marrow and capped with cartilaginous structures. The cortices (compact bone) which surround the marrow cavity contains sheets of mineralized bone surrounding blood vessels (Haversian canals), with the outermost sheet corresponding to the oldest, most mature bone. Connecting the walls of the tubes are finer structures, known as trabeculae, or woven bone. While the cortices provide most of the mechanical strength to the long bones, the flat bones, such as those in the skull or ribs, have a very thin cortex filled with woven bone, hence that woven bone provides a great deal more strength. The trabeculae bone in the cortices also contributes to the strength, as it provides struts that share the load applied to the bones, and it is these elements that disappear in conditions associated with bone fragility (increased tendency to fracture) such as osteoporosis.

Each type of bone consists primarily of mineral (a microcrystalline analogue of the geologic mineral hydroxyapatite) and an extracellular matrix (predominately type I collagen). The chemical formula of hydroxyapatite mineral is $Ca_{10}(PO_4)_6(OH)_2$, but physiologic mineral found in both bones and teeth is poorly crystalline, and contains many lattice vacancies and substitutions [6] so that chemical analysis of the calcium/phosphorus ratio of bone is generally not equal to the predicted 1.67:1. Depending on diet and type of bone (cortical/trabecular), how much it remodels, what its functions are, etc., the most common substituents are carbonate (which substitutes for both phosphate and hydroxyl ions in the lattice [7], magnesium, fluoride, strontium, and citrate [8].

The organic matrix of bone is mainly type I collagen, a fibrous protein that provides the tissue with elasticity and flexibility, and also serves as the template upon which the mineral is deposited. There are three types of cells within the bone, osteoblasts, which are bone forming cells, osteocytes, which formerly were osteoblasts, but once surrounded by mineral take on the function of communication and responsiveness to load, and bone remodeling cells, or osteoclasts [9]. The matrix also contains about 5% noncollagenous proteins. These proteins [10] regulate both the structure and function of the tissues and their component cells, and the process of mineralization. As discussed below, we have used mutant mice in which one or more matrix proteins were ablated (knockouts, KO), or overexpressed (transgenic, TG) to characterize the effects of these proteins on bone using IR imaging and IR microspectroscopy. Studies of the effects of these proteins in mutants lacking enzymes that modify them [11], or mutants having abnormal enzyme expression, have indicated the importance of matrix modification for mineralization [12–14]. In addition to the extracellular matrix proteins, there are also lipids, both within the cell membranes, inside the cell, and within the matrix. The properties of the lipids in bones and teeth were reviewed elsewhere [15].

3. Infrared spectroscopic imaging of bone properties

The properties of bone that determine its mechanical strength (and hence bones most important functional characteristic) are its geometry (shape and connectivity), whether it contains flaws (such as micro-cracks [16]), and its material properties [17]. These material properties include mineral content, mineral and matrix composition, cellular activity, and distribution of crystal sizes [18]. Most of these material properties with the exception of cellular activity can be determined by infrared microscopy and infrared microscopic imaging.

As discussed throughout the reviews in this volume, the paradigm shift that occurred when an array detector was coupled with an infrared microscope, enabling multiple spectra to be collected from the same type of tissue sections that were

Table 1
Parameters used in the IR analysis of mineralized tissues

Parameter	Region analyzed (cm^{-1})
Mineral (phosphate ν_1, ν_3)/matrix (amide I) peak area ratio	900–1200/1585–1720
Carbonate (ν_2)/phosphate (ν_1, ν_3) peak area ratio	860–890/900–1200
Carbonate (ν_2)/amide I peak area ratio	860–890/1585–1720
Fractional Carbonate A substitution	I_{872}/860–890
fractional Carbonate B substitution	I_{878}/860–890
Crystallinity	Peak area 1030/1020 or I_{1030}/I_{1020}
Acid phosphate content	Peak area 1117/900–1200 or I_{1117}/I_{960}
Collagen maturity	Peak area 1660/1686 or I_{1660}/I_{1690}

I = intensity at wavenumber indicated.

Table 2
IR analyses of long bones of mutant and transgenic mice

Animal model	Finding relative to WT	Reference
Type X collagen transgenic	No bone or cartilage phenotype	[25]
Osteocalcin KO	Cortical bone increased mineral content, decreased crystal size	[26]
Matrix glia protein KO	Trabecular mineral content increased, crystal size increased	[27]
Biglycan KO	Cortical & Trabecular bone—decreased mineral content, increased crystal size	[28]
Osteopontin KO	Increased mineral content, increased crystal size	[29]
Osteonectin KO	Increased mineral content, increased crystal size	[30]
Dentin matrix protein 1 KO	Decreased mineral content, increased crystal size	[31]
Tissue non-specific alkaline phosphatase KO	Decreased mineral content	[12,13]
IGF-binding protein 5, TG	Lower mineral content—no change in crystal size	[32]
Vitamin D receptor TG	No change in mineral properties	[33]
TGF-beta KO	Decreased mineral content, decreased crystal size	[34]

Table 3
IR parameters in tibias of α-galactosidase (Fabry) KO mice and WT controls

	Min/Matrix	1030/1020	1660/1690
Proximal			
Cortex Fabry	7.55±1.29	1.29±0.03 *	1.81±0.31
WT	6.47±1.01	1.23±0.07	1.75±0.14
Distal Cortex			
Fabry	8.94±0.23 **	1.30±0.02	1.73±0.16
WT	9.79±0.75	1.30±0.03	1.84±0.18
Trabeculae			
Fabry	8.07±1.07	1.19±0.04	1.59±0.14
WT	7.57±0.69	1.17±0.04	1.65±0.18

* $P<0.10$ vs. WT based on Student's t-test.
** $P<0.05$ vs. WT based on Student's t-test.

routinely used for histology and immunohistochemistry, but without the need for destructive staining. Fig. 1 shows a typical spectrum taken from the cortex of a healthy wildtype mouse bone. The absorbances of interest are illustrated here and their origin for bone analyses is listed in Table 1. For studies using infrared microscopy and imaging, the samples have to be sufficiently thin to allow the transmittance of light. For this purpose the bone must be sectioned with a microtome, generally using a diamond knife. When the studying sections of bone, to insure that there are no variations because the sections were not cut uniformly, the general practice is to express all parameters as ratios. The IR parameters that have been validated for imaging of bone include the mineral/matrix ratio (the ratio of the integrated v1,v3 phosphate band/amide I band) that is linearly related to the mineral (ash) content of mixtures of hydroxyapatite and collagen [19,20], the carbonate/phosphate ratio that is related to the chemically determined extent of carbonate substitution, the 1030/1020 peak height ratio, that is related to the crystallite size in the long (c-axis) dimension as determined by X-ray diffraction line broadening [21], and the peak height ratios for the different types of carbonate substitution [22]. In addition, we have defined a parameter that is related to the maturity of the collagen fibrils [23] and to the extent of collagen cross-linking in the section being examined, although the precise chemical composition of the contributing cross-links remains to be elucidated. Also, although used less frequently to look at bone, relevant parameters can be obtained from the 2853/2890 lipid/protein ratio [24] and a variety of absorbance ratios used to characterize DNA and sulfate constituents of tissues that will not be discussed here.

The findings of our analyses of transgenic, knockout, and diseased human bones were recently reviewed in detail [4,5] and are summarized in Table 2. To illustrate the techniques and demonstrate the types of information that can be acquired from IR imaging spectroscopy of bone, we will discuss one mouse model from which the data have not previously been reported, and indicate how infrared imaging spectroscopy was

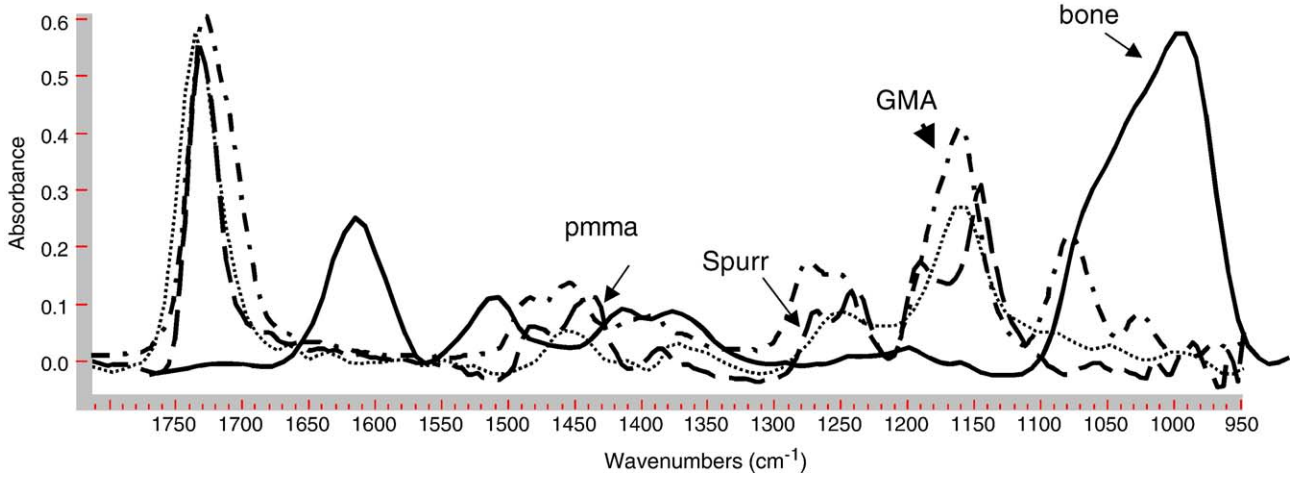

Fig. 2. Unsubtracted bone spectra in tissues fixed in glycolmethacrylate (GMA), and the spectra of the individual embedding media, Spurr, polymethylmethacrylate (PMMA) and glycolmethacrylate (GMA).

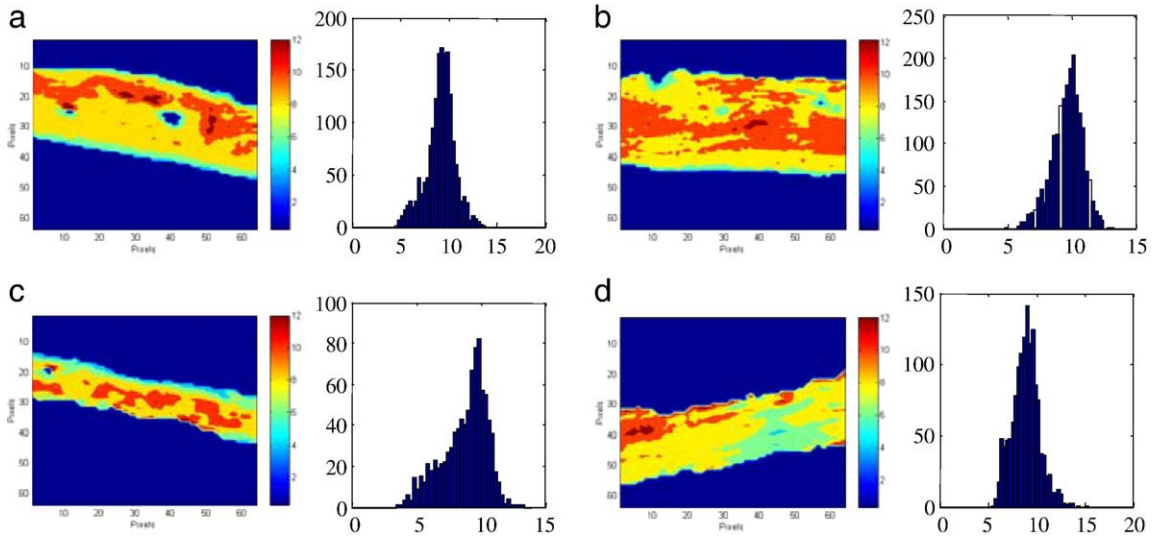

Fig. 3. Typical image and pixel distribution of mineral:matrix content in proximal (a, c) and distal (b, d) cortical bone of WT (a, b) and Fabry's (c, d) mice tibia. Pixel numbers are shown on the x and y axes; 1 pixel = 6.25 um.

used to determine whether there were bone changes in these animals.

4. Analysis of Fabry's and wildtype mice bones

A deficiency in the lysosomal hydrolase-galactosidaseA (α-gal A; EC 3.2.1.22) leads to impaired catabolism of -galactosyl-terminal lipids such as globotriaosylceramide (Gb3). Individuals with this deficiency have vascular occlusions that cause cardiovascular, cerebrovascular, and renal disease [35,36], and there have been some suggestions that bone disease is also involved [37–40]. However, since the condition is associated with many complicating factors, there have been no detailed analyses of bone in Fabry disease. A few cases involving avascular necrosis (AVN) of the femoral head have been reported, and recently in one case report the presence of trihexose ceramide in both the normal and necrotic bone was found based on lipid analyses [40].

Oshima et al. [41] reported the development of mice lacking galactosidase A. These mice accumulate Gb3 (ceramide-trihexoside) in their liver and kidneys as early as at 10 weeks of age. We performed infrared imaging analysis on the bones of these animals, and age-, background-, and sex-matched controls to determine whether there were any detectable bone abnormalities.

Bones of three male KO and four male wildtype (WT) animals at 8 weeks of age were examined by infrared imaging using a BioRad Infrared Imaging System (BioRad, Cambridge,

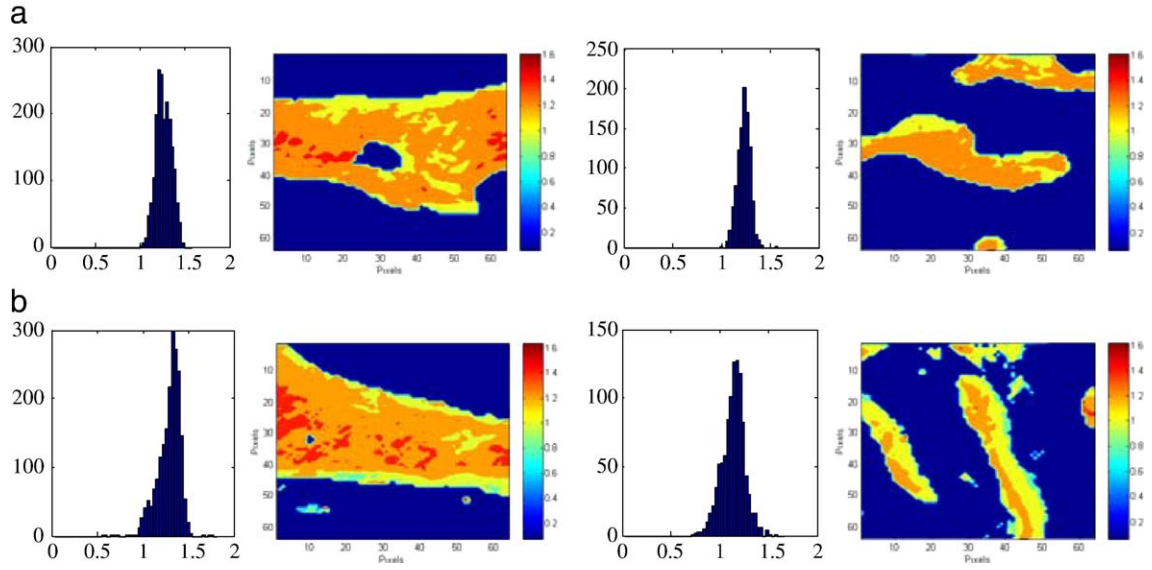

Fig. 4. Image and pixel distribution of crystallinity parameter in cortical (left) and trabecular (right) bone of WT (a) and Fabry's mice (b) tibia.

MA). To analyze bone by infrared imaging, thin sections (1–6 μm thick) are required. Since bone is a hard tissue, it is difficult to cut, even with a diamond knife, thus for sectioning it must be embedded in an even harder substance [42]. For the study of the Fabry mice bones, because we were trying to preserve lipids, we compared embedding in Spurr's medium, polymethylmethacrylate (PMMA) and glycolmethyacrylate (GMA) (Fig. 2). While all three embedding media had spectra that did not overlap the majority of the mineral bands GMA had less interference in the areas of lipid analyses. Sections 3–4 um thick were used for all analyses.

After collection of data from multiple areas (400 μm× 400 μm) in the cortex, trabecular bone, and epiphysial growth plate (the cartilaginous area from which long bone growth and development commences), the GMA contribution was subtracted from all the spectra using Isys software (Spectral Dimensions, Olney MD), and the mineral/matrix ratio, 1030/1020 ratio, and 1660/1690 ratios were calculated using the same software as described elsewhere [30]. The BioRad detector did not allow collection of 870 cm^{-1} data for analyses of carbonate content. A lipid (methylene)/protein (methyl) ratio was also calculated using Isys. Images of each parameter using the same color scale were generated in Isys, and pixel histograms for each parameter produced. Means and standard deviations for each parameter were calculated, and compared among animals using ANOVA (Table 3).

The mineral/matrix ratio (Fig. 3, Table 3) was not significantly different when the Fabry's bones were compared to the WT in the proximal cortical and trabecular bone, however the Fabry distal cortex, which represents older bone had a lower mineral/matrix ratio than the WT. Typical pixel histograms are shown along with their respective images for each parameter. There was a tendency ($P=0.06$) for the crystallinity to be increased in the Fabry proximal end of the cortical bone relative to the WT proximal cortices, while both the ends of the cortical bone in the Fabry mice had a tendency to be higher in crystallinity (crystal size/perfection) than the WT proximal bone. In the trabeculae, the crystallinity was not significantly increased in the Fabry's bones as compared to the WT, however the distributions were consistently sharper (Fig. 4, Table 3). The collagen maturity (1660/1690 ratio) was not altered in any of the sites examined (Table 3). Imaging suggested that there were a few pixels with elevated lipid/protein ratio in the Fabry bones that were not seen in the WT (data not shown).

The absence of large differences in the mineral properties of the bones of these animals may reflect the similar lack of major bone phenotype in human patients with Fabry's disease, and may also be related to the developmental age of these animals. It is interesting to note that there was also no significant dental phenotype in the Fabry mice at 5 weeks [43]. This too may be related to developmental age, as the cerebrosides accumulate with age, and a similar accumulation in the vascularity of mineralized tissues may take a greater time to develop. Based on studies of transgenic mice overexpressing α-galactosidase A, it does not appear that the enzyme is expressed in bone cells, although it is expressed in bone marrow [44], which may also explain the lack of phenotype.

The results, however do illustrate how infrared imaging microscopy can be applied to the analyses of bones in metabolic diseases, as well as in KO and TG and osteoporotic tissues.

5. Conclusions and perspective

Infrared spectroscopic imaging has changed the way bone phenotype can be characterized. While the Fabry mice described here did not show many significant changes in their bone mineral properties, changes in matrix properties were readily defined. Future studies will need to look at older mice, and the mechanical properties of these bones. However, the quantitative information achievable from this technique, as opposed to the qualitative information that is obtained with the use of special stains is immediately apparent. The limitation, of course, is the need to embed and section the tissues. Dr. Nancy Camacho, who has another chapter in this volume, is probing the use of near IR to examine the surface of bone through skin, hence without the need to sacrifice, let alone embed the bone. Dr. Ed Draper, similarly is developing non-invasive Raman spectroscopy [45] using a pico-second Kerr gate that enables data to be required 1 mm below the skin. These techniques may, in the future, enable imaging spectroscopy without the need for biopsies, but the additional information that can be obtained by infrared and Raman imaging will continue to provide important insight into the bone changes and how they are related to the presence and absence of specific bone cell and matrix molecules and the treatments for different bone diseases.

Acknowledgements

Dr. Boskey's work as described in this review was supported by NIH grants DE04141 and AR041325. Dr. Gomez's work was supported by grants PR02-0128 and RED G03-122 Instituto Carlos III. Fabry mouse work was supported by the Division of Intramural Research, National Institute of Dental and Craniofacial Research, NIH. The imaging data were collected at the NIH sponsored Core Facility at the Hospital for Special Surgery (AR046121) . This investigation was conducted in a facility constructed with support from Research Facilities Improvement Program Grant Number C06-RR12538-01 from the National Center for Research Resources, National Institutes of Health.

References

[1] S. Majumdar, A review of magnetic resonance (MR) imaging of trabecular bone micro-architecture: contribution to the prediction of biomechanical properties and fracture prevalence, Technol. Health Care 6 (1998) 321–327.
[2] D. Hans, T. Fuerst, T. Lang, S. Majumdar, Y. Lu, H.K. Genant, C. Gluer, How can we measure bone quality? Bailliere's Clin. Rheumatol. 11 (1997) 495–515.
[3] A.L. Boskey, Mineral analysis provides insights into the mechanism of biomineralization, Calcif. Tissue Int. 72 (2003) 533–536.
[4] A. Boskey, R. Mendelsohn, Infrared analysis of bone in health and disease, J. Biomed. Opt. 10 (2005) 031102–031109.

[5] A.L. Boskey, R. Mendelsohn, Infrared spectroscopic characterization of mineralized tissues, Vibr. Spectrosc. 38 (2005) 107–114.
[6] N.C. Blumenthal, F. Betts, A.S. Posner, Formation and structure of Ca-deficient hydroxyapatite, Calcif. Tissue Int. 33 (1981) 111–117.
[7] G. Penel, G. Leroy, C. Rey, E. Bres, MicroRaman spectral study of the PO4 and CO3 vibrational modes in synthetic and biological apatites, Calcif. Tissue Int. 63 (1998) 475–481.
[8] J. Green, The physicochemical structure of bone: cellular and noncellular elements, Miner. Electrolyte Metab. 20 (1994) 7–15.
[9] T. Kobayashi, H. Kronenberg, Minireview: transcriptional regulation in development of bone, Endocrinology 146 (2005) 1012–1017.
[10] J. Gokhale, P.G. Robey, A.L. Boskey, The Biochemistry of Bone, in: R. Marcus, D. Feldman, J. Kelsey (Eds.), 2nd Ed., Osteoporosis, vol 1, Academic Press, San Diego, 2001, pp. 107–189.
[11] N.P. Camacho, C.M. Rimnac, R.A. Meyer Jr., S. Doty, A.L. Boskey, Effect of abnormal mineralization on the mechanical behavior of X-linked hypophosphatemic mice femora, Bone 17 (1995) 271–278.
[12] H.C. Anderson, D. Harmey, N.P. Camacho, R. Garimella, J.B. Sipe, S. Tague, X. Bi, K. Johnson, R. Terkeltaub, J.L. Millan, Sustained osteomalacia of long bones despite major improvement in other hypophosphatasia-related mineral deficits in tissue nonspecific alkaline phosphatase/nucleotide pyrophosphatase phosphodiesterase 1 double-deficient mice, Am. J. Pathol. 166 (2005) 1711–1720.
[13] H.C. Anderson, J.B. Sipe, L. Hessle, R. Dhanyamraju, E. Atti, N.P. Camacho, J.L. Millan, Impaired calcification around matrix vesicles of growth plate and bone in alkaline phosphatase-deficient mice, Am. J. Pathol. 164 (2004) 841–847.
[14] L.C. Gowen, D.N. Petersen, A.L. Mansolf, H. Qi, J.L. Stock, G.T. Tkalcevic, H.A. Simmons, D.T. Crawford, K.L. Chidsey-Frink, J.D. McNeish, T.A. Brown, Targeted disruption of the osteoblast/osteocyte factor 45 gene (OF45) results in increased bone formation and bone mass, J. Biol. Chem. 278 (2003) 1998–2007.
[15] M. Goldberg, A.L. Boskey, Lipids and biomineralizations, Prog. Histochem. Cytochem. 31 (1996) 1–187.
[16] Y.N. Yeni, D.P. Fyhrie, A rate-dependent microcrack-bridging model that can explain the strain rate dependency of cortical bone apparent yield strength, J. Biomech. 36 (2003) 1343–1353.
[17] M.L Bouxsein, Non-invasive measurements of bone strength: promise and peril, J. Musculoskelet. Neuronal. Interact. 4 (2004) 404–405.
[18] R.D. Blank, T.H. Baldini, M. Kaufman, S. Bailey, R. Gupta, Y. Yershov, A.L. Boskey, S.N. Coppersmith, P. Demant, E.P. Paschalis, Spectroscopically determined collagen Pyr/deH-DHLNL cross-link ratio and crystallinity indices differ markedly in recombinant congenic mice with divergent calculated bone tissue strength, Connect. Tissue Res. 44 (2003) 134–142.
[19] D. Pienkowski, M.T. Doers, M.-C. Monier-Faugere, N.P. Camacho, A.L. Boskey, H.H. Malluche, Inferior mechanical properties, lower bone mineral densities, and altered mineral structure of canine bones after calcitonin treatment, J. Bone Miner. Res. 12 (1997) 1936–1943.
[20] D. Faibish, A. Gomes, G. Boivin, I. Binderman, A. Boskey, Infrared imaging of calcified tissue in bone biopsies from adults with osteomalacia, Bone 36 (2005) 6–12.
[21] S.J. Gadaleta, E.P. Paschalis, F. Betts, R. Mendelsohn, Fourier transform infrared spectroscopy of the solution mediated conversion of amorphous calcium phosphate to hydroxyapatite: new correlations between X-ray diffraction to infrared data, Calcif. Tissue Int. 58 (1996) 9–16.
[22] D.G. Nelson, J.D. Featherstone, Preparation, analysis, and characterization of carbonated apatites, Calcif. Tissue Int. 34 (1982) S69–S81.
[23] E.P. Paschalis, K. Verdelis, S.B. Doty, A.L. Boskey, R. Mendelsohn, M. Yamauchi, Spectroscopic characterization of collagen cross-links in bone, J. Bone Miner. Res. 16 (2001) 1821–1828.
[24] R. Mendelsohn, G. Anderle, M. Jaworsky, H.H. Mantsch, R.A. Dluhy, Fourier transform infrared spectroscopic studies of lipid–protein interaction in native and reconstituted sarcoplasmic reticulum, Biochim. Biophys. Acta. 775 (1984) 215–224.
[25] E.P. Paschalis, O. Jacenko, B. Olsen, B. deCrombrugghe, A.L. Boskey, The role of type X collagen in endochondral ossification as deduced by Fourier transform infrared microscopy analysis, Connect. Tissue Res. 35 (1996) 371–377.
[26] A.L. Boskey, S. Gadaleta, C. Gundberg, S.B. Doty, P. Ducy, G. Karsenty, Fourier transform infrared microspectroscopic analysis of bones of osteocalcin-deficient mice provides insight into the function of osteocalcin, Bone 23 (1998) 187–196.
[27] A.L. Boskey, G. Karsenty, M.D. McKee, Mineral characterization of bones and soft tissues in matrix glia protein deficient mice, in: M. Goldberg, A. Boskey, C. Robinson (Eds.), Chemistry and Biology of Mineralized Tissues, Am. Acad. Orthopaed. Surgeons, Chicago, IL, 2000, pp. 63–67.
[28] T. Xu, L. Fisher, P. Bianco, G. Longnecker, A.L. Boskey, E. Smith, J. Bonadio, S. Goldstein, C. Zhao, P. Dominguez, A.M. Heegaard, K. Satomura, P. Gehron-Robey, A. Kulkarni, B. Sommer, M. Young, Targeted disruption of the biglycan gene leads to osteoporosis in mice, Nat. Genet. 20 (1998) 78–86.
[29] A.L. Boskey, L. Spevak, E. Paschalis, S.B. Doty, M.D. McKee, Osteopontin deficiency increases mineral content and mineral crystallinity in mouse bone, Calcif. Tissue Int. 71 (2002) 145–154.
[30] A.L. Boskey, D.J. Moore, M. Amling, E. Canalis, A.M. Delany, Infrared analysis of the mineral and matrix in bones of osteonectin-null mice and their wildtype controls, J. Bone Miner. Res. 18 (2003) 1005–1011.
[31] Y. Ling, H.F. Rios, E.R. Myers, Y. Lu, J.Q. Feng, A.L. Boskey, DMP1 depletion decreases bone mineralization in vivo: an FTIR imaging analysis, J. Bone Miner. Res. 20 (2005) 2169–2177.
[32] E. Atti, A.L. Boskey, E. Canalis, Overexpression of IGF-binding protein 5 alters mineral and matrix properties in mouse femora: an infrared imaging study, Calcif. Tissue Int. 76 (2005) 187–193.
[33] B.M. Misof, P. Roschger, W. Tesch, P.A. Baldock, A. Valenta, P. Messmer, J.A. Eisman, A.L. Boskey, E.M. Gardiner, P. Fratzl, K. Klaushofer, Targeted overexpression of vitamin D receptor in osteoblasts increases calcium concentration without affecting structural properties of bone mineral crystals, Calcif. Tissue Int. 73 (2003) 251–257.
[34] E. Atti, S. Gomez, S.M. Wahl, R. Mendelsohn, E. Paschalis, A.L. Boskey, Effects of transforming growth factor-beta deficiency on bone development: a Fourier transform-infrared imaging analysis, Bone 31 (2002) 675–684.
[35] S.C. Garman, D.N. Garboczi, Structural basis of Fabry disease, Mol. Genet. Metab. 77 (2002) 3–11.
[36] E. Schaefer, A. Mehta, A. Gal, Genotype and phenotype in Fabry disease: analysis of the Fabry Outcome Survey, Acta Paediatr., Suppl. 94 (2005) 87–92.
[37] E. Fischer, Fabry disease, a disease with rheumatic aspects: radiology of soft tissue and bone changes in the hand, Z. Rheumatol. 45 (1986) 36–41.
[38] D.P. Germain, K. Benistan, P. Boutouyrie, C. Mutschler, Osteopenia and osteoporosis: previously unrecognized manifestations of Fabry disease, Clin. Genet. 68 (2005) 93–95.
[39] Y.H. Lien, L.W. Lai, Bilateral femoral head and distal tibial osteonecrosis in a patient with Fabry disease, Am. J. Orthop. 34 (2005) 192–194.
[40] H. Horiuchi, N. Saito, S. Kobayashi, H. Ota, T. Taketomi, K. Takaoka, Avascular necrosis of the femoral head in a patient with Fabry's disease: identification of ceramide trihexoside in the bone by delayed-extraction matrix-assisted laser desorption ionization-time-of-flight mass spectrometry, Arthritis Rheum. 46 (2002) 1922–1925.
[41] T. Oshima, G.J. Murray, W.D. Swaim, G. Longenecker, J.M. Quirk, C.O. Cardarelli, Y. Sugimoto, I. Pastan, M.M. Gottesman, R.O. Brady, A.B. Kulkarni, Á-galactosidase A deficient mice: a model of Fabry disease, Proc. Natl. Acad. Sci. U. S. A. 94 (1997) 2540–2544.
[42] S. Aparicio, S.B. Doty, N.P. Camacho, E.P. Paschalis, L. Spevak, R. Mendelsohn, A.L. Boskey, Optimal methods for processing mineralized tissues for Fourier transform infrared microspectroscopy, Calcif. Tissue Int. 70 (2002) 422–429.
[43] M. Goldberg, D. Septier, A. Limaye, T. Sreenath, A.B. Kulkarni, Dentin and enamel phenotype in Fabry mice, Oral Biosci. Med. 4 (2005) 265–271.
[44] M. Hoshikawa, R. Kase, M. Tadokoro, H. Sakuraba, T. Sakiyama, Long-term expressed human alpha-galactosidase A in tissues of HalphaG transgenic mice, Pediatr. Int. 46 (2004) 673–677.
[45] E.R. Draper, M.D. Morris, N.P. Camacho, P. Matousek, M. Towrie, A.W. Parker, A.E. Goodship, Novel assessment of bone using time-resolved transcutaneous Raman spectroscopy, J. Bone Miner. Res. 20 (2005) 1968–1972.